Colloid & Polymer Science Colloid Polym Sci 272:910–932 (1994)

Structure transfer from a polymeric melt to the solid state Part III: Influence of knots on structure and mechanical properties of semicrystalline polymers

R. K. Bayer

Institut für Werkstofftechnik
Universität Gh Kassel, FRG

Abstract. Investigations of the influence of crystallization conditions and molecular weight on mechanical properties of melt spun monofilaments have been carried out in previous studies [1, 2].

The present results emphasize the influence of crystallization upon two classes of molecular entanglements present in the melt:

1) mobile entanglements with short life times;
2) long living knots as a superstructure of the entanglement network

On the other hand, it is shown that the former number of entanglements controls the thickness of the crystalline lamellae. It is pointed out that knots also have a specific influence on morphology. Knots form the amorphous phase of a semicrystalline polymer and are mechanically active. The present model is comparatively discussed in light of Peterlin's plastic deformation model and Kilian's van der Waals Network Theory.

Key words: Polyethylene – melt spinning – mechanical properties – crystallization – entanglements – knots

1. Introduction

1.1. Influence of temperature on crystallization

It is well known that morphology of semicrystalline polymers develops during crystallization on cooling from the melt. Crystallization does not begin immediately, when decreasing the temperature just below the melting point, but after a certain undercooling. The nucleation rate in the vicinity below the melting point is not very high, and increases by further lowering the temperature. Crystal growth rate also influences the morphology of the developing crystallinity. Growth rate decreases by decreasing the temperature because of the lower molecular mobility. From both contributions, an optimum crystallization temperature can be selected below the melting point [1].

The obtained morphology (i.e., lamellar thickness) is essentially characterized by the degree of undercooling, i.e., by the crystallization temperature [2–4]. The influence of the structure of the melt on crystallization is negligible, if crystallization is carried out at the optimum crystallization temperature.

1.2. Quenched semicrystalline polymers

In case of quenching of the melt to room temperature, certain parallelisms between the structure of the melt and the structure of the solid state have been drawn. Fischer [5] has shown, for instance, that in spite of the crystallization process involved when a polymer melt is quenched, the radius of gyration of a molecular coil does not change. At lower degrees of undercooling, this is no longer valid, in this case significant molecular

motions of the chain molecules are involved, giving rise to a more perfect crystallization [1–4] which leads to an increase of the radius of gyration, measured in the solid state. Fischer describes the resulting morphology upon quenching as *Erstarrungsmodell* (instant solidification) [6, 7].

Rault et al. [8–12] measured long periods L of polyethylene and polyethyleneterephtalate samples, which were quenched from the melt. The state of the melt was varied by choosing different molecular weights, as well as by changing the melt temperature. These authors observed that L changes systematically with the state of the melt. Rault attributes these changes in L to a variation of the molecular random coil radius. Accordingly, an increase of the coil radius of the melt yields a growth of the long period. This is confirmed in case of experiments carried out on flexible chains (PE, PP, PA), in which the coil radius decreases with increasing temperature, which results in a decrease of the long period. In contrast, in the case of stiff chains (PB, PEO), the coil radius increases with melt temperature while the long period of the quenched materials shows a parallel increase.

Variations of molecular weight seem to underline, as well, the relation between the radius of the random coil and long period. The larger the coil radius owing to higher molecular weight, the larger becomes the long period of the quenched melt.

Crystal thickness of the quenched samples is relatively little affected by the change of melt structure. Taking into account that long period L is equal to the sum of the average crystal thickness (l_c) and the thickness of the amorphous layers l_a, then the thickness of the amorphous phase should correlate with variation of the melt structure, as summarized here in the coil radius.

Generally, the amorphous phase is correlated to the presence of entanglements of the melt. For example, Fischer [5] concludes that due to the few movements of chain molecules during crystallization in the quenching process (coil radius remains unchanged), entanglements of the melt should be preserved. The entanglements are accordingly concentrated in the amorphous interlayers. Kilian [13] bases his crystallization theory on a similar concept. The thickness of the crystalline lamellae is defined by the distance between densely entangled amorphous interlayers [13, 14].

The experiments of Katayama [15] show more directly the influence of entanglements on crystallization. Here, the time scale of the crystallization process, beginning at the melt temperature, has been transformed to a spatial scale by means of the melt spinning process. Near the die the extruded strand is in the melt state, while somewhat further away from the die it solidifies. Most interesting is the fact that small-angle-x-ray scattering develops before wide-angle x-ray diffraction. This means that, before the melt shows a well-ordered crystal structure (WAXS), there arise electron density fluctuations, characterizing the existence of a periodicity at small scattering angles. Before crystallization, already a periodic layer structure of regions with lower and increased electron density is formed in the melt. Correspondingly, layers of low electron density where entanglements must be concentrated are formed. Immediately before crystallization, entanglements are forced to leave the regions where crystallization will develop.

Summarizing the above cited results, one can conclude that the amorphous thickness l_a on one hand is given by $\sqrt{M}$ (coil radius), and on the other hand by the entanglement concentration. Hence, the entanglement concentration should be controlled by $\sqrt{M}$. Entanglement concentration in the melt however does not change above the critical entanglement molecular weight M_c. Because entanglement concentration is not changed by crystallization [5, 13], this also holds for the solid state. Hence, it cannot be the entanglement concentration itself which controls l_a.

In parts I and II of this series [16, 17] a superstructure of the entanglements called knots is presented. If two chains entangle with each other, they form a pair of entangled chains. In fact, many more chains do participate in such a string of entanglement-meshes (interpenetrating entanglement-meshes). When the length of the chains reaches a critical value (critical molecular weight $M_c' \approx 10^5$ for polyethylene), the pairs of entangled chains can entangle with each other (Circles in Fig. 1). We shall call "knots" to these second order entanglements. They represent the superstructure of the entanglement network. The knot is a multi-chain coupling. While an entanglement is formed by two chains a knot consists of many more chains (Fig. 1).

The knots considerably reinforce the structure of the entanglement-network. It is much easier to disentangle a chain from the entanglement-network when knots do not exist. The ivy-plant gives

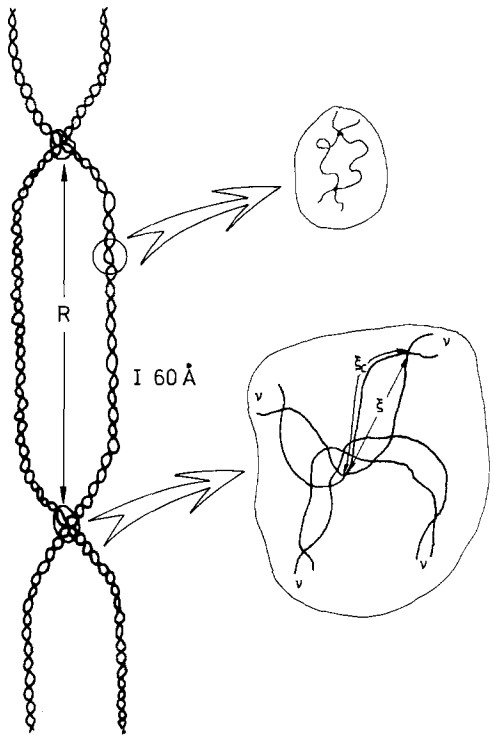

Fig. 1. Schematic drawing of a knot mesh as super structure of the entanglements: Entangled strands of chain molecules (entanglement mesh chain) entangle with each other. A magnification of a knot is plotted on the right side. The parameter ν symbolizes the interpenetration of an entanglement mesh (by ν other segments of entanglement meshes (s_c). Distance from knot to knot = R. Curvilinear distance from knot to knot = $s_c' = \nu \cdot s_c$.

a very instructive example for the formation of knots [18]. If one cuts from the entangled tendrils of the plant a defined length which is not too large it is easy to disentangle the plants. If, however, a critical length (when entangled tendrils entangle with each other) is surpassed it is very difficult to separate one tendril from the bundle. This critical length corresponds to the above-mentioned molecular weight M_c'. Since knots are formed in the melt they are transferred to the solid state on cooling (crystallization). The density of knots can be increased by molecular weight [17]. Above the critical molecular weight M_c' the density of the knots remains constant. The aim of the present paper is to correlate the amorphous thickness with the knots. For this purpose the crystallization (cooling) conditions during melt spinning have been varied. Mechanical (elastic recovery, elongation at break) and structural (crystalline and amorphous thickness) properties which show the influence of knots have been measured.

2. Experimental

Monofilaments of polyethylene were produced by melt spinning at different crystallization conditions by changing the temperature and the position of a cooling bath. The thread passes through this bath after leaving the die of the extruder. Table 1 indicates the variation of the cooling conditions. The material used in this investigation was a linear PE with molecular weight $M_\eta = 152\,000$ (Hostalen GF 5250) which was extruded through a 0.5 mm die at a melt temperature of 185 °C. Extrusion speed was kept constant at $v_0 = 4$ m/min. Table 1 includes a quantity cooling gradient, which characterizes the temperature decrease from the melt (185 °C) to a given bath temperature at a given distance bath-die. Furthermore, draft was varied by changing the drawdown speed of the melt spinning apparatus. Additional melt spinning experiments were carried out with a PE- sample with a lower molecular weight $M_\eta = 56\,000$ (Vestolen A 6016). The produced monofilaments were characterized by density measurements, carried out with an isopropylalcohol-dioxane density gradient column and birefringence measurements, using an optical microscope with calcite compensator. The elongation at break λ_B of the monofilaments was measured by tensile test experiments, using a gauge length of 10 cm and a crosshead speed of 50 mm/min. Elastic recovery (ER_x)

$$ER_x = \frac{\Delta l_{tot} - \Delta l_{rest}}{\Delta l_{tot}} \cdot 100\% ,$$

where Δl_{tot} is the total deformation of a sample with initial length $l_0 = 20$ cm and Δl_{rest} is the length corresponding to remnant plastic deformation measured after 2 min, was measured as well.

Reference will also be made to measurements of density and x-ray long period of linear unoriented polyethylenes with varying molecular weight [19]. These samples were prepared from the melt state using a hot press. One series of samples was slowly crystallized (S-series), while another series

Table 1. Cooling conditions at the Melt Spinning Process

Series number		Cooling gradient from melt to solidification in °C/mm
1	The monofilament is cooled by ambient air. At a distance of 150 mm behind the die, the molten strand solidifies.	0.4
2	Water bath temperature: 78 °C Distance die-bath: 15 mm	7.2
3	Water bath temperature: 78 °C Distance die-bath: 1 mm	107
4	Water bath temperature: 4 °C Distance die-bath: 1 mm	181

Table 2. Viscosimetric average molecular weight of the materials investigated

Material	M_η
Lupolen 6031 M	52–000
Vestolen A 6016	58–000
Vestolen A 6013	88–000
Rigidex 6006–60	115–000
Hostalen GF5250	151–000
Lupolen 6021 D	161–000
Lupolen 5661 B	173–000
Lupolen 5261 Z	248–000
Hostalen GR6255	307–000
Hostalen GUR	ca. 1000–000

of samples was quenched (Q-series). Table 2 shows the materials used for these samples.

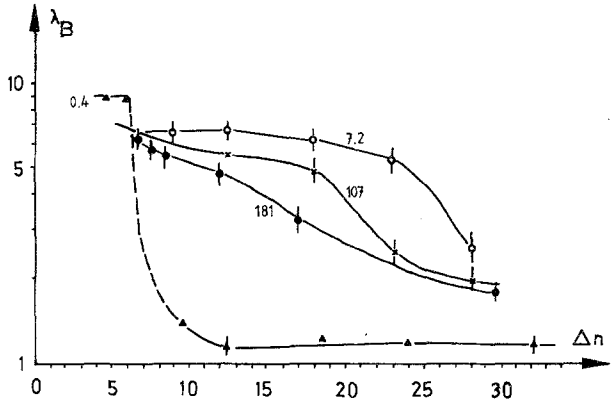

Fig. 2. Elongation at break of monofilaments of Hostalen GF 5250 against birefringence. Cooling gradient (°C/mm) is varied (see Table 1) Die diameter 0.5 mm

3. Results

Figure 2 represents the variation of the elongation at break λ_B as a function of birefringence for different cooling conditions. Figure 3 represents the densities of these series of monofilaments. It is seen that density is independent of orientation. The highest density value was obtained for the slowest cooling rate from the melt. Figures 2 and 3 show that both extensibility λ_B and density decrease simultaneously with increasing cooling rate, i.e., the higher the density of the samples, the higher the measured extensibility. The only exception to this parallel behavior of these two quantities is due to a transition from ductile to brittle behavior occurring for samples with the lowest cooling rate having high crystallinity and elevated

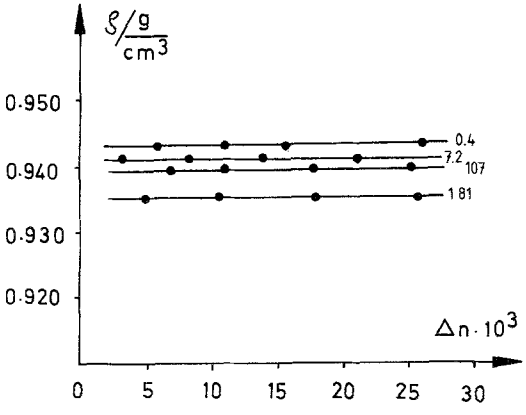

Fig. 3. Densities of the series of Hostalen GF 5250 monofilaments corresponding to the cooling gradients of Table 1. Die diameter: 0.5 mm

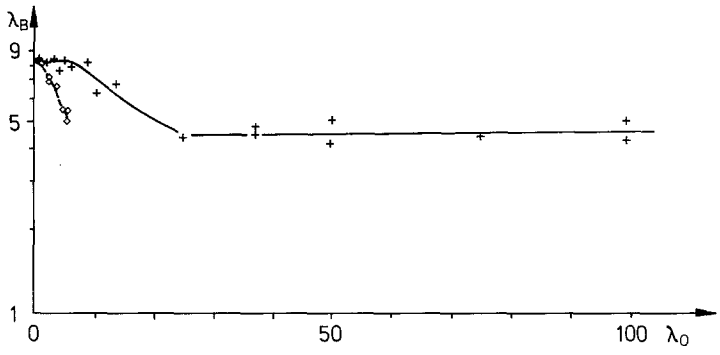

Fig. 4. Elongation at break of monofilament meltspun from a low molecular weight – PE (M_η = 58 000). Squares: quenched in a 4° water bath 1 mm behind the die, crosses: slowly cooled at ambient air. Die diameter: 0.25 mm x-axis: draft λ_0 = drawdown velocity/extrusion speed

orientation (Fig. 2). Figure 4 shows the influence of cooling conditions on elongation at break λ_B for melt spun monofilaments at the lower molecular weight grade sample. One can see that quenching decreases considerably λ_B like observed above for the higher molecular weight material (Fig. 2). Furthermore, the maximum draft (spinnability) is much lower for the quenched than for the slowly cooled monofilaments. Figures 5 and 6 illustrate the elastic recovery of these series of melt spun samples for initial deformation of 10 and 15% respectively. By comparing Figs. 4 and 5 with Fig. 3, one observes that in both cases elastic recovery decreases with increasing density (crystallinity).

Figure 7 shows the dependence of the elastic recovery ER_x on the preceding initial deformation x. The relative elastic recovery decreases steadily, with increasing initial deformation.

Three principal regions of elongation can be distinguished.

1) the zone of high elastic recovery up to $x = 15\%$;
2) $15\% < x < 110\%$.
   Here, ER_x decreases slowly, with initial elongation x.
3) $x > 110\%$.
   $x = 110\%$ characterizes the formation of the neck zone, i.e., the transition to the fibrillar state. This yields a larger decrease of elastic recovery.

Figure 8 shows the variation of λ_B against birefringence obtained during the meltspinning process. Figure 8 illustrates the influence of annealing on the λ_B vs Δn curves for a series of samples spun at a higher crystallization rate. It is noteworthy that the increase of crystallinity (increase of density, see legend of Fig. 8) due to an annealing process has no influence on λ_B of these series of

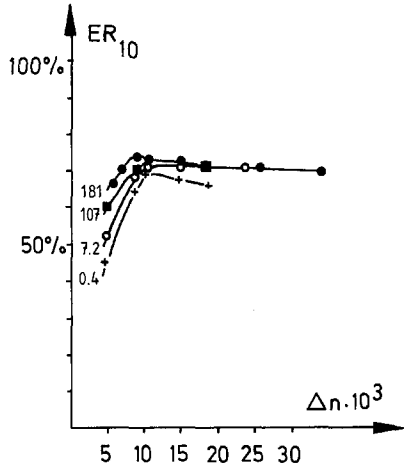

Fig. 5. Elastic recovery after 10% elongation of an initial monofilament length 10 = 20 cm. Dependence on birefringence. Cooling gradient as shown in Table 1. Die diameter: 0.5 mm

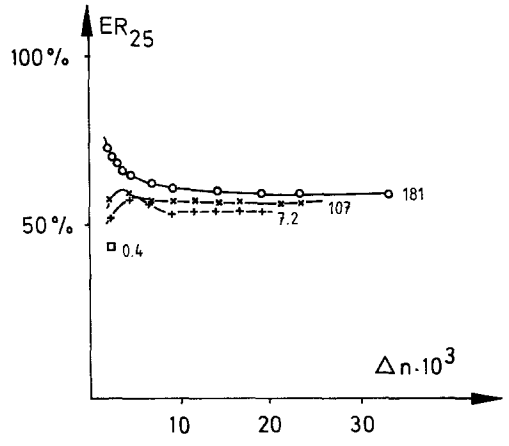

Fig. 6. Elastic recovery after 25% elongation of an initial monofilament length l_0 = 20 cm. Dependence on birefringence. Cooling gradient of Table 1. Die diameter: 0.5 mm

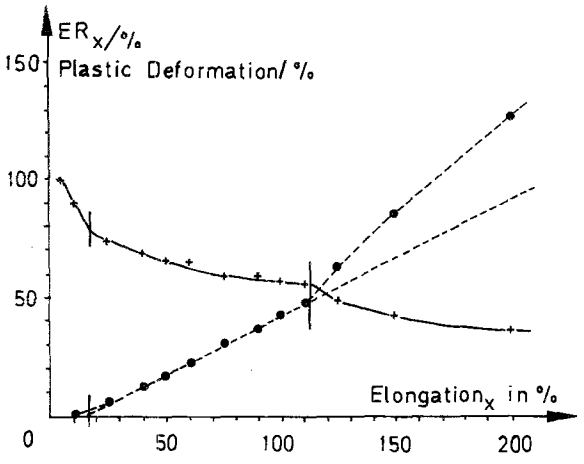

Fig. 7. Elastic recovery ER_x against deformation x before retraction. Dotted line: plastic deformation. The plastic deformation is counted in percent of the original length ($\langle 100\% - ER_x \rangle \cdot x(\%)/100\%$). Material: Hostalen GF 5250, Extrusion conditions: 40 °C water bath, 1 mm distance die-bath, 0.25 mm die diameter, $v_0 = 1$ m/min, $T_m = 185$ C, $\lambda_0 \approx 1$

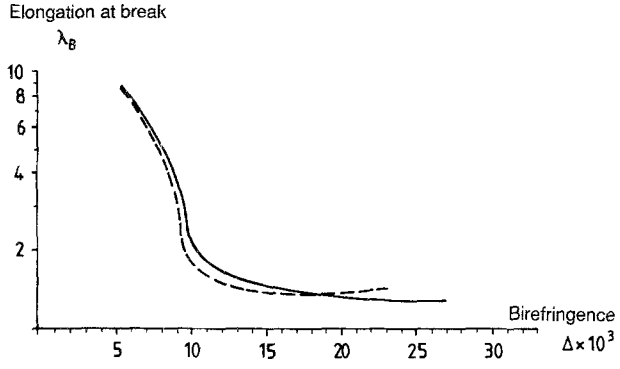

Fig. 8. Embrittlement by annealing: λ_B against birefringence. Material: Hostalen GF 5250, extrusion conditions: 4 °C water bath, 1 mm distance bath-die, $T_m = 170$ °C, $v_0 = 1$ m/min, die = 0.25 diameter, solid line: as spun ($\rho = 0.933$ g/cm^3) dotted line: annealed for 2 h at 117 C in N_2 atmosphere ($\rho = 0.948$ g/cm^3)

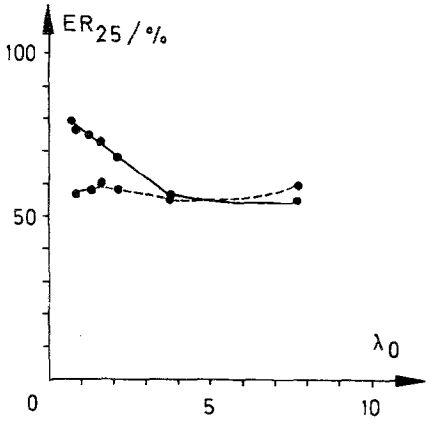

Fig. 9. Elastic recovery ER_{25} versus draft λ_0. For material and processing conditions see Figs. 7, 8

Table 3. Morphology of the quenched polyethylenes (Q-Series)

M	L/Å	l_a/Å	l/Å
52 000	188	72	116
58 000	185	74	111
88 000	198	84	114
115 000	208	90	118
161 000	208	90	118
173 000	212	93	119
248 000	229	108	121
307 000	236	112	124
ca. 1000–000	279	161	118

Table 4. Morphology of the Slowly Cooled Polyethylenes (S-Series)

M	b/Å	L/Å	l_a/Å	l/Å
52 000	126	296	66	230
58 000	157	281	70	211
88 000	179	311	80	231
115 000	193	323	82	241
161 000	220	334	87	247
173 000	223	340	89	251
248 000	224	375	108	267
307 000	225	376	114	262

monofilaments. Figure 9 shows that elastic recovery for these series of samples notably decreases due to the annealing process.

Tables 3 and 4 show the long period L and the crystalline (l_c and amorphous thickness (l_a) of the unoriented sample of the linear polyethylenes with varying molecular weight. The results have been obtained from x-ray and density measurements (see also [20]).

Figure 10 show the increase of l_a with molecular weight. At a critical molecular weight of 170 000, one observes a stronger increase rate of l_a with M_η. The crystal thickness also increases linearly with M_η (Fig. 10). At the same critical molecular weight l_c reaches a saturation value. This leveling-off value [14] has been correlated to a saturation value of entanglements in the crystal surfaces.

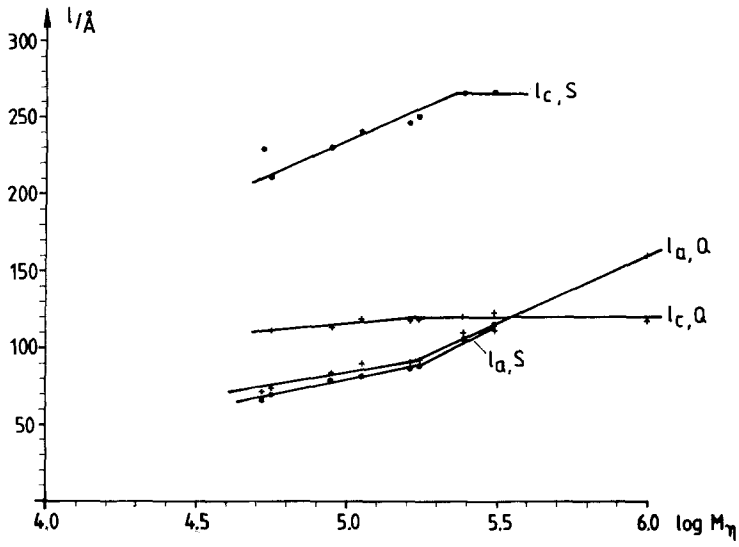

Fig. 10. Average thickness of the amorphous layers l_a and the crystalline lamellae l_c in isotropic polyethylenes dependent on mean molecular weight. Different cooling conditions: (Q = Quenched, S = slowly cooled see Tables 3, 4), Commercial materials (see Table 2)

4. Discussion

4.1. Crystallization induced unknotting

The results for elongation at break (Fig. 2) cannot be interpreted solely on the basis of the influence of crystallization conditions, because the rheology of the melt spinning process is varied simultaneously in a part of the experiments (series numbers 1 – 3 in Table 1). Since crystallization rates are connected to an increased drawdown length l (distance bath-die), the deformation time of the melt $t \sim l/v_0$ also increases with this parameter. Due to an increased t/τ-ratio (τ = mean relaxation time of the melt) the number of knots will decrease [17], which contributes to an increase of λ_B. The larger the deformation time, the higher the number of knots that will fluctuate in the melt spinning process. The large changes in the maximum draft λ_{0B} (spinnability) (from 100 cooling by air to 10 with the cooling bath directly behind the die) as well as in λ_B (Fig. 4) can be attributed to the phenomenon of the relaxation of knots of the low molecular weight grade PE. In the case of series number 1 – 3 (Table 1) the described change of rheology is superimposed to the variation of crystallization rate. The influence of crystallization on λ_B is revealed if cooling conditions of 107 and 181 °C/mm (at constant l) (Table 1) are compared.

Here, the rheology conditions (distance die-bath) are kept constant, while crystallization temperature is strongly changed (78 °C to 40 °C). In good agreement with the results of Ward [21] for isotropic PE, the material with higher crystallinity yields a better extensibility independently of orientation (Fig. 2). However, the increase of crystallinity through annealing does not cause any remarkable change on λ_B (see Fig. 8). Crystallinity itself is not the critical physical parameter which influences the value of the elongation at break. Instead, the process of crystallization from the melt is the one which determines λ_B. The values of λ_B are small when the material is quenched from the melt, and it increases systematically by improving crystallinity from the melt.

In parts I and II of this series [16, 17] it was shown that λ_B was related to the number of knots transferred from the melt into the solid state. In light of this concept, crystallization from the melt induces a λ_B increase which can be explained in terms of a reduction of the number of knots.

Hence, there should exist a crystallization induced unknotting * mechanism. In a similar sense,

*) Crystallization induced unknotting is a different mechanism from elongation induced unknotting which may occur during plastic deformation. Kilian [22] has pointed out that the van der Waals network of LDPE samples widens during elongation. If the density of knots before elongation is reduced by crystallization the sample will be unknotted more easily by further elongation. In any case, the double influence on knot density has been separated in this work. Thus, deformation was kept constant, while the influence of crystallization from the melt will be the point to be discussed in what follows (see Fig. 2).

Rault [12] speaks of disentanglement by crystallization. From the evaluation of microhardness measurements [13, 19] it can be shown, however, that the entanglement density is not changed by crystallization.

The hypothesis of a crystallization induced unknotting has been confirmed directly from the existence of different critical molecular weights M'_c for the percolation threshold of knots when crystallization conditions are changed. In [19] we have shown from hardness measurements that a critical thickness of the amorphous phase $l'_{ac} = 90$ Å describes the percolation criterion of the knots in a better way than any other percolation criterion. On the other hand, the amorphous thickness of quenched polyethylene is always a little larger than in the case of slowly crystallized polyethylene (Fig. 10). This implies that $l_{ac} = 90$ Å for a series of quenched linear PE's of varying mean molecular weight is reached at a lower critical molecular weight than for well-crystallized polyethylenes.

M'_c (quenched series) $< M'_c$ (slowly – crystallized series); more experimental evidence is given in [23].

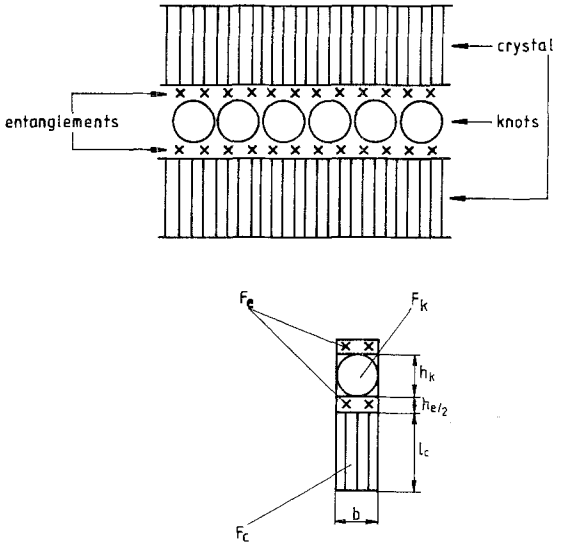

Fig. 11. Schematic drawing of the structure of the amorphous layers. The unit cell of the knot-network is indicated below. b = width of the unit cell; l_c = crystal thickness, area of the crystal = $b \cdot l_c$; h_k = knot thickness, area of the knot $F_k = h_k \cdot b$; $h_e/2$ = thickness of the entanglement layer on the crystal surface; cross-sectional area of the crystal surface $F_e = b \cdot h_e$

This implies an unknotting process by crystallization. In the case of slow crystallization of the melt higher mean chain length than for quenched PE's is necessary in order to reach the percolation threshold of knots.

While crystallization can hardly change the density of entanglements, knots as a superstructure of entanglements are the first elements to suffer under the microscopic force fields due to developing crystallization.

Crystallization-induced unknotting is especially observed at $M_w < M'_c$. In this region of molecular weights large differences in the elongation at break of well-crystallized and quenched PE are observed [21], [23]. When the percolation of knots is reached above $M'_c = 10^5$ knot density cannot be changed any more by crystallization. Elongation at break of the quenched material for $M > M'_c$ does not differ very much [21, 23] from elongation at break of well-crystallized material.

At this point, crystallization models as mentioned in the introduction should be modified. The role of the knots on the structure of semicrystalline polymers will be discussed.

4.2. A model of crystallization: general features

Crystallization of polymer melts is restricted by the entanglement network. Entanglements are such large defects that they cannot be incorporated into the regular three-dimensional crystal structure. Thus, only segments of chain molecules in the interior of an entanglement-mesh can be aligned parallely, thus contributing to the crystal growth. During crystallization, entanglements are pushed aside by the growing crystals. When crystallization stops, zones enriched with entanglements form the amorphous zones and entanglements are concentrated on the crystal surfaces [13].

Due to the larger size of the knots as compared with that of entanglements, it is obvious that knots can not be incorporated into the growing crystals, contributing, as a result, to the emerging amorphous zones. From the above considerations a model of the semi-crystalline structure of polymers could be visualized as follows (Fig. 11).

As mentioned above, crystallization parallelly aligns the parts of chain molecules within the meshes of the entanglement network. The crystallization process should include all entanglement

meshes. Hence, all entanglements should lie on crystal surfaces.

Kilian [24] estimates the average diameter of an entanglement to be about 15 Å. Amorphous thicknesses as shown in Fig. 10 are, however, thicker than would correspond to two entanglement-layers (30 Å). This indicates that also entanglement-meshes within the center of the amorphous layers must exist. Knots might act as stabilizing factor for these entanglements. On the other hand, entanglement-meshes which belong to the superstructure of a knot cannot crystallize (Fig. 11). In what follows, we will attempt to describe in more detail the coarse features of the model of Fig. 11. The beginning of crystallization leads to microscopic force fields which will be directed towards the strongest elements of the melt which we call knots. Crystallization may deform the knots as mentioned above (4.1), though it is not probable that knots are pushed along great distances. This is confirmed by neutron-scattering experiments of Fischer [6] which show that the radius of the coil measured in the melt remains nearly unaffected by crystallization.

The mean distance between the knots is given by

$$R = \alpha\sqrt{\nu \cdot M_c} = s_c \qquad (1)$$

(see sec.4.3.2, 4.3.3, [17]),
where ν is Rault's Degree of interpenetration of entanglement meshes;

M_c = critical entanglement molecular weight
$M_c' = \nu \cdot M_c$
= critical knot molecular weight
s_c = distance along the chain between entanglements
α = chain flexibility .

As mentioned above, the mean distance $R = s_c$ between knots should not be changed too much by crystallization. On the other hand, entanglement meshes are completely stretched upon a good crystallization pushing the entanglements onto the crystal surfaces and incorporating the stretched chain-segments with a length s_c into the crystal (see Fig. 11). Maximum crystal thicknesses of $l_c = 270$ Å $\approx s_c$ (277 Å) can be obtained in this way for $M_w > M_c'$ (Fig. 10). There is only one possibility to achieve this stretching process without substantially affecting the position of the knots. Upon crystallization the chain of entangled meshes illustrated in Fig. 1 involves a folding process that deposits the entanglements on the crystal surface. In this model the "entanglement mesh chain" is transformed upon crystallization into the structure of Fig. 12, where the distance between the knots is increased slightly above $R = s_c$. The mean distance between entanglements increases however from 61 [25] to 270 Å. This simple model also explains why crystal thickness cannot overcome a critical thickness of $l_c = 270$ Å (see saturation level of l_c in Fig. 10). Otherwise, Fig. 12 exhibits another interesting feature: Only two out of $\nu = 27$ entanglement-meshes of the knot mesh Figs 1, 12) may have contact to a knot.

A further argument, also in support of the existence of a folded (stretched) entanglement mesh chain within lamellar crystals is the following: The model of Fig. 12 refers to a monomolecular layer of crystallizing chain molecules. The chain molecules of this simplified picture are thought to have a distance d_c which also is the thickness of the monomolecular layer. The cross-section of such a molecule in the monomolecular layer is thus $d_c^2 \cdot d_c$ can be estimated from the unit cell of the orthorhombic crystalline lattice of PE as shown in Fig. 13:

$$b \cdot a = 2d_c^2 ,$$

where a, b are th dimensions of the unit cell.

$$d_c = \sqrt{\frac{b \cdot a}{2}} = 4.26 \text{ Å}$$

The diameter of an entanglement of 15 Å [24] precludes the formation of entanglements on the crystal surface between adjacent chains of the crystal.

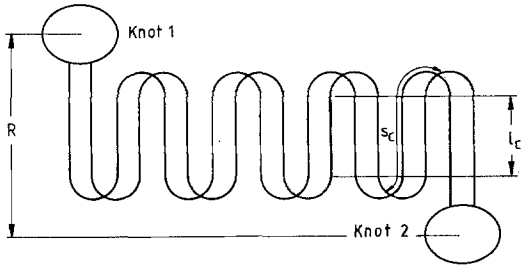

Fig. 12. Schematic drawing of the formation of a crystal by folding an entanglement-mesh chain (as plotted in Fig. 1)

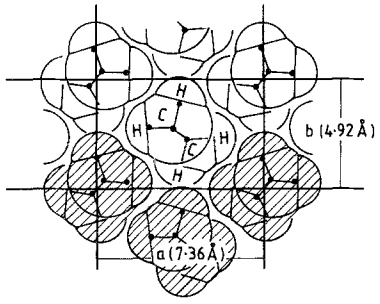

Fig. 13. Unit cell of polyethylene. Shadowed molecules represent the average thickness d_c of the molecular cross-section d_c^2 of a molecule within the crystalline phase

Consequently, the arc which forms half of the entanglement length has to be connected to the overnext chain of the crystal (see Fig. 12). In this case there is room enough for a second chain to cross over the first chain folded segment. The diameter of this entanglement (composed by the crossing over of two chain segments) is equal to 3×4.25 Å ≈ 13 Å, which is roughly in agreement with Kilian's estimation [24]. The folded entanglement mesh chain of Fig. 12 fulfills such a requirement for entanglement formation. Hence, during crystallization entanglements can be transported easily from the melt (Fig. 1) to the crystal surface by a simultaneous mechanism of stretching and disinterpenetration of the entanglement-meshes and by means of folding of the entanglement mesh chain.

4.3. Relations of describing harmonic superstructures in an amorphous melt

4.3.1. The extensibility of an entanglement-mesh: In order to derive the extensibility λ_c of an entanglement mesh, we make the following "*Gedankenexperiment*". We consider the situation of an entanglement-mesh in the melt state: the mesh is v-fold interpenetrated by other molecular chain segments having the length s_c. The v-fold interpenetrated entanglement-mesh has a statistical conformation. Now, we begin to take off the s_c-segments in the interior of the mesh, one after another. The density of the material within the mesh is considered to remain constant. Thus, the diameter of the reference entanglement-mesh will shrink while the mesh is simultaneously stretched (Fig. 14).

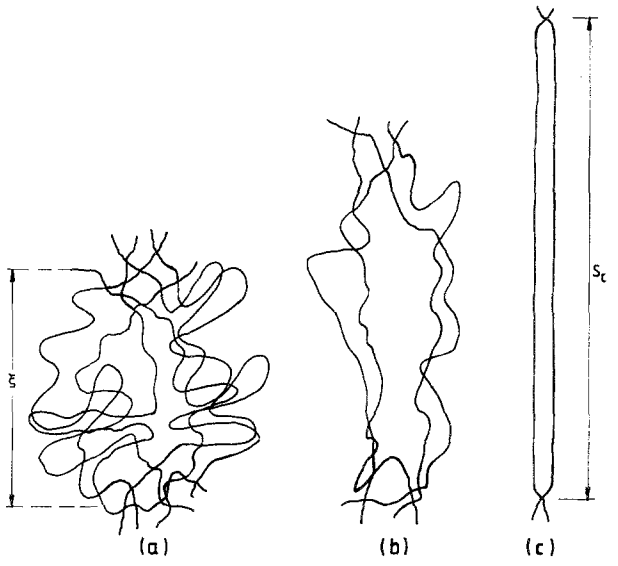

Fig. 14. Schematic drawing relating extensibility λ_c of an entanglement mesh with the degree of interpenetration left side (a): v taken as 6, three interpenetrating entanglement meshes of statistical shape are drawn. Chain density is kept constant when entanglement-meshes are taken out (b) and (c). Due to constancy of density the mean distance between entanglements increases from (a): ξ to (c): s_c

Figure 14 shows that v independent steps lead from an isotropous entanglement-mesh of statistical conformation to a completely stetched entanglement-mesh. As a consequence, it may be written:

$$\lambda_c = \sqrt{v} \,. \tag{2}$$

Taking $v = 27$ which is an average value from the results presented by Rault [25] for different polymers, it follows:

$$\lambda_c = 5.2 \,.$$

On the other hand, the extensibility of an entanglement mesh is given by the ratio of the length of the completely extended mesh (s_c) to the initial statistical mesh diameter (ζ) (s_c, and ξ see Fig. 14):

$$\lambda_c = \frac{s_c}{\zeta} \,. \tag{3}$$

Rault [25] has summarized s_c and ζ-values for various thermoplastic materials. Applying Eq. (3) λ_c-values for various polymers can be calculated from these data. Values between 5 and 8 are obtained.

Equation (2) implies that the chain between two entanglements consists of v independent statistical chain-segments with a length l_s.

Hence, the chain length between entanglements s_c (Fig. A-2) can be expressed as

$$s_c = v l_s \,, \tag{4}$$

while for the diameter of the isotropous entanglement-mesh, it follows that

$$\zeta = \sqrt{v} l_s \,. \tag{5}$$

Inserting Eqs. (4, 5), into (3), we get Eq. (2). This shows the consistency of Eqs. (3–5) with (2).

Equation (4, 5) are the basis of the following considerations.

4.3.2. Formulae for critical entanglement molecular weight M_c and statistical chain-segment l_s: For ζ also holds [25]

$$\zeta = \alpha\sqrt{M_c} \,, \tag{6}$$

with α being the chain flexibility.

The contour length between adjacent entanglements is given by

$$s_c = M_c \cdot l_u / M_u \,, \tag{7}$$

l_u and M_u being the projected length (1.27 Å) and the relative molecular mass (14) of the repeating CH_2-unit.

From

$$s_c/\zeta = \lambda_c = \sqrt{v} = \frac{M_c \cdot \frac{l_u}{M_u}}{\alpha\sqrt{M_c}} \,, \tag{8}$$

We deduce for the critical entanglement molecular weight

$$M_c = \alpha^2 v \cdot (M_u/l_u)^2 \,. \tag{9}$$

The critical entanglement molecular weight is given by two parameters only: chain flexibility (α) and relative molecular mass per repeating C–C unit M_u/l_u.

If we combine Eqs. (4), (6), and (9), we obtain for the statistical chain-segment:

$$l_s = \alpha^2 M_u / l_u \,. \tag{10}$$

4.3.3. Knot meshes as superstructure of entanglement meshes: The critical molecular weight of the knots [17] is given by

$$M_c' = v \cdot M_c \,, \tag{11}$$

from which follows

$$s_c' = v^2 \cdot l_s \,. \tag{12}$$

The diameter of the knot mesh, similar to Eq. (5), is given by

$$R = \alpha\sqrt{M_c'} \,. \tag{1}$$

Inserting (9) and (10) yields

$$R = v l_s = s_c \,. \tag{13}$$

Analogously to Eq. (3) the deformability of a knot mesh is defined as:

$$\lambda_c' = s_c'/R \,. \tag{14}$$

Inserting Eq. (12, 13), one obtains:

$$\lambda_c' = v \,. \tag{14a}$$

Now, we consider the total deformability of the knot-mesh λ_c' as product of two independent contributions (deformability of the entanglement-mesh λ_c and deformability λ_k of the knot-mesh consisting of undeformable entanglement-meshes (blobs of the diameter ζ) [26]:

$$\lambda_c' = \lambda_c \cdot \lambda_k \,. \tag{15}$$

Then, we obtain from Eq. (14a):

$$\lambda_k = \sqrt{v} = \lambda_c \,. \tag{16}$$

This means that "there are v blobs of the size ζ between 2 adjacent knots. The distance between knots is then $R = \sqrt{v}\zeta$ [26] " (see Eqs. (5, 13)). This means that a knot-mesh as superstructure of entanglement-meshes exhibits the same behavior as an entanglement-mesh as super structure of the statistical chain segment. The respective deformabilities are equal (Eq. (16)) and reflect equivalent statistical elements of a blob (ζ) and a statistical chain segment (l_s).

4.3.4. Relation between chain flexibility α and amorphous density ρ_a: Due to the v-fold interpenetration of an entanglement-mesh, we can write for the van der Waals-volume V_c of a chain with the molecular weight M_c:

$$V_c = \frac{\zeta^3}{v} \,. \tag{17}$$

which leads to

$$V_c = \sqrt{v} \cdot l_s^3 \,. \tag{18}$$

The diameter d_a (of a random coil in the amorphous phase) can be derived from:

$$V_c = d_a^2 \cdot s_c = d_a^2 \cdot v \cdot l_s \,. \tag{19}$$

Using Eqs. (18) and (19):

$$d_a = v^{-1/4} \cdot l_s \,. \tag{20}$$

The value of d_a in the amorphous phase is related to the thickness d_c in the crystalline phase through:

$$\left(\frac{d_a}{d_c}\right)^2 = \frac{\rho_c}{\rho_a} \tag{21}$$

ρ_c = density of the crystals
ρ_a = density of the amorphous
(a molecule, independent of whether it belongs to the crystalline or to the amorphous phase, exhibits the same length, but it has different effective diameters).

By combining Eqs. (20) and (21) an expression for l_s can be derived which by Eq. (7) allows to calculate the chain flexibility α:

$$\alpha = \sqrt{\frac{\rho_c}{\rho_a}} \cdot d_c \cdot v^{1/4} \Big/ \frac{M_u}{l_u} \,. \tag{22}$$

4.3.5. Comparison with experimental values: The above relations show how the structure parameters of the melt s_c, s'_c, and R are characterized by the statistical chain-segment l_s which is given by one relevant parameter: the chain flexibility α. This parameter α may easily be calculated from the amorphous density ρ_a (Eq. (22)). Hence, from the value of α all structural features may be derived straightforwardly using Eqs. (4, 5, 10, 12, 13, 20).

If the above equations are applied for polyethylene ($l_u = 2.54$ Å, $M_u = 28$, $\rho_c = 1.00$ g/cm^3; ρ_a ($T = 20\,^\circ$C) $= 0.89$ g/cm^3) [27], $v = 27$, we obtain:

$$\alpha(20\,^\circ\text{C}) = 0.96 \frac{\text{Å}}{\sqrt{g}}$$

$$d_c = 4.26 \text{ Å}$$

$$d_a = 4.52 \text{ Å}$$

$$M_c = 3050$$

$$s_c = 277 \text{ Å} = R$$

$$l_s = 10.3 \text{ Å}$$

$$M'_c = 83\,380.$$

The α, M_c, and M'_c data are consistent with the values known from the literature:

$$\left(\alpha = 0.95 \frac{\text{Å}}{\sqrt{g}}\right) \text{[25]}$$

$(M_c = 3200)$ [25]

$(M'_c \approx 10^5)$ [23, 28] .

The latter value, however, depends strongly on processing conditions and molecular weight distribution and will be the subject of another paper [23]. Because of the above-mentioned good correspondence with experimental values, it turns out that $v = 27$ represents a good approximation.

Only the length of the statistical chain segment ($l_s = 10.3$ Å) of an entangled melt is somewhat lower than that calculated from Flory's $c_{N\infty}$-value

$$\bar{l}_s = \frac{l c_{N\infty}}{\cos_{\alpha/2}}$$

$\alpha = 180\,^\circ -$ Bond angle
$= 180\,^\circ - 109.5\,^\circ$
$= 70.5\,^\circ$
$l = 1.54$ Å (Bond length) [28]

$$\bar{l}_s = 1{,}87 \text{ Å } c_{N\infty} \tag{23}$$

$$c_{N\infty} = 6{,}87$$

$$\bar{l}_s = 12{,}8 \text{ Å} \,.$$

Our l_s- value which is derived from Eq. (10) is confirmed not only by the experimental α-value but also by the calculated one (Eq. (22)). Our l_s-value describes a resting melt which is characterized by the parameters v and α.

This means that a real network of chain molecules has a somewhat more flexible statistical unit than an isolated chain which is the basis for Flory's $c_{N\infty}$ value. The mechanically effective $\bar{l}_s$-unit is equal to 8 CH_2-units (see also appendix 2) while Flory's $\bar{l}_s$-value comprises 10 CH_2-units. When $l_s = 10{,}3$ Å is inserted in Eq. (23) it yields $c_N = 5{,}51$. Following [29] (Fig. 9, Chapter V, therein) this corresponds to an interaction of $N \approx 27 = v$ CH_2-groups. The reduced length of the mechanically effective statistical chain segment is characterized by the interaction of the CH_2-groups along a chain length of only of $v \cdot l_u$ and not $n \cdot l_u$, where $n \geq 200$ characterizes Flory's value of $C_{N\infty} = 6{,}87$.

In Appendix 1 an attempt is made to explain the physical importance of the chain length $v \cdot l_u$.

4.4. Quantitative description of a semi-crystalline polymer including knots

4.4.1. Functionality of a knot: Let R^2 be area of the "unit cell" of the knot-network in the two-dimensional model. Figure 15 schematically depicts this two-dimensional model.

The volume of a monomolecular polymer layer will then be given by

$$R^2 d_a = y d_a^2 , \tag{24}$$

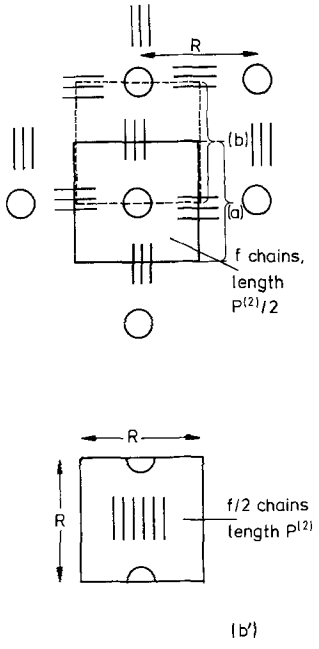

Fig. 15. Schematic drawing of the unit cell of the knot network. Knots are symbolized as circles. Three straight lines represent chains of the length $P^{(2)}$ that connect the knots:

a) is the unit cell of the knot network which is the basis of Eq. (27). The unit cell contains an f-functional knot which has arms of a length of $P^{(2)}/2$;
b) is an equivalent version of the unit cell;
b') is a simplification developed from (b) which is the basis of the model of Fig. 17

Here, two knot halves are interconnected by f/2 chains of the length of $P^{(2)}$. In every case (a, b, b',) the unit cell contains a total chain length of

$$y = \frac{f \cdot P^{(2)}}{2}$$

(see Eq. (26))

and the total length y of the polymer chains within the unit cell of the knot network will be

$$y = R^2/d_a . \tag{25}$$

The total length y of the polymer chains is distributed on the f-branches of the f-functional knot, i.e.,

$$y = f \cdot P^{(2)}/2 , \tag{26}$$

where $P^{(2)}$ is the chain length between two knots projected into the monomolecular layer.

The value of $P^{(2)}/2$ is used because the unit cell of the two-dimensional knot-network is given by the half-distance from knot to knot (see Fig. 15). From Eqs. (25) and (26), it follows:

$$P^{(2)} \cdot f = 2\frac{R^2}{d_a} , \tag{27}$$

$P^{(2)}$ can easily be calculated if $P^{(3)}$ (three-dimensional knot network projection) and $P^{(1)}$ (one-dimensional knot network projection) are also considered. Thus,

$$P^{(3)} = v \cdot s_c = v^2 \cdot l_s \tag{28}$$

$$P^{(1)} = R = s_c = v \cdot l_s . \tag{29}$$

Similarly for $P^{(2)}$, it follows that

$$P^{(2)} = v^{3/2} \cdot l_s = \sqrt{v} \cdot s_c . \tag{30}$$

Hence, in our model, we use a shortened chain with the length $P^{(2)}$ in the two-dimensional area. In the real case this chain is much longer because it statistically passes through the three-dimensional space.

From Eqs. (27) and (30), we obtain the functionality of the knot in a monomolecular layer as:

$$f = 2\frac{R^2}{d_a v^{3/2} \cdot l_s} . \tag{31}$$

By substituting Eqs. (13) and (20) in Eq. (31), one obtains

$$f = 2v^{3/4} \approx 24 . \tag{32}$$

A similar calculation yields for the functionality of a knot in the three-dimensional space (based on Eq. (28))

$$f = 2v^{3/2} \approx 280 . \tag{33}$$

On the basis of the calculated data Fig. 16 shows a model of the semi-crystalline structure.

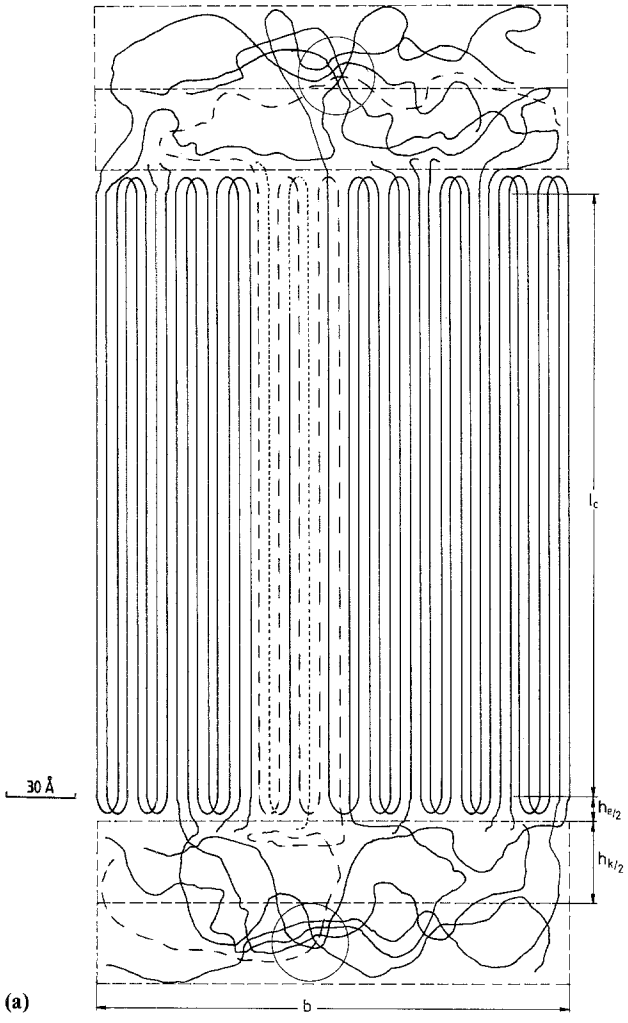

The "unit cell" is shown here as two half knots which are interconnected by $f/2$-chains which have a length of $P^{(2)}$ (see Fig. 15 b'). This is equivalent to a unit-cell which would show f-chains with a length of $P^{(2)}/2$ (Fig. 15a). Only half of the amorphous layer is shown in Fig. 16a. The knot-forming entanglement-mesh chain belonging to the neighboring unit cell is not shown (half knot of Fig 15b').

Figure 16b shows a reflection of the amorphous structure of Fig. 16a along its center line (dashed line) which gives an impression of an interpenetrating entanglement mesh chain belonging to the neighboring unit cell.

Figure 16a represents the classical situation of the percolation. The mean chain length is long enough ($P^{(2)} = 5\ s_c$) to connect one knot to another. In Fig. 16a we show 10 chains with 5 s_c-units from which 4 s_c-units contribute to the crystal and 1 s_c-unit contributes to one knot half. Five molecules contribute to the upper knot half while the other five molecules contribute to the lower knot half. A 7 s_c molecule which is shown off in Fig. 16 connects the knots. Finally, a 3 s_c-molecule (shown off as dotted line) which contributes only to the crystal is taken into account to compensate the overlength of the 7 s_c-molecule. The force-bearing centers of the knots are symbolized as circles in the center of the amorphous phase. Twelve chains go out of the circles, which indicates the functionality $f/2 = 12$ of a knot half.

Fig. 16(a). Drawing of the two-dimensional projection of the unit cell of the knot-network. Corresponding to Fig. 15b' the unit cell is formed by $f/2 = 12$ chains which on average are $P^{(2)} = 5\ s_c$-units long. s_c is the curvilinear distance between entanglements. One molecule (dashed line) is 7 sc units long; one molecule (pointed line) is 3 sc units long; the other 10 molecules (solid lines) are 5 sc units long. A knot arc (center of the amorphous phase) is composed of six pairs of entanglement-meshes with a reduced curvilinear distance between entanglements $s_k = s_c/2$ ($s_c = 277$ A). The knot center is indicated by a circle. The interpenetrating knot-forming entanglement mesh chain is not shown. An impression of how the complete amorphous phase would then look like is given in Fig. 16b which is obtained from the knot arcs of Fig. 16a by reflection along the center line of the amorphous phase. Width of the unit cell $b = 212$ A; crystal thickness $l_c = 268$ A; thickness of the entanglement layer on the crystal surface $h_e/2 = 8$ A; thickness of the amorphous phase $l_{ac} = h_k + h_e = 90$ A (See Sec. 4.4.3).

4.4.2. Calculations of the morphological parameters: According to Fig. 11, we observe within the unit cell of the knot network three partial areas which correspond to the area of the knot F_k, the area F_e of the entanglement layer which represents a cut through the surface of a crystal, and the area of the crystal F_c. All these areas sum to R^2 which is the area of the unit cell of the knot-network:

$$F_k + F_e + F_c = R^2 \,. \tag{34}$$

These three partial areas can be estimated as follows:

$$F_c = l_c \cdot b \,, \tag{35}$$

where b

$$b = \underbrace{f/2 \cdot (P^{(2)}/s_c - m)}_{\text{number of parallel chains in the crystal.}} \cdot d_c, \tag{36}$$

m describes the number of s_c-units of these projected chains with the length $P^{(2)}$ which remains in the knot. $m = 2$ describes the knot model of Fig. 1. Two entanglement meshes form a loop which is entangled by two meshes of another entanglement chain, thus forming the knot. The contour length s_k of an entanglement mesh within the knot would then be $s_k = s_c$. Thus, a value of $m = 2$ would guarantee that the dimension of the knot should not be changed by crystallization of the length s_c. The case $m = 1$ describes that the entanglement-chain makes one fold of the length s_c more (see Fig. 12) and thus increases the width b of the crystal. Consequently, for the length of the chain between entanglements within the knot $s_k = s_c/2$. This case would correspond to a crystallization-induced disknotting (like experimentally observed). The model of the crystal as folded entanglement-mesh-chain implies that the disknotting process occurs in a discrete step. The area of the knot

$$F_k = f s_k d_a \,, \tag{37}$$

due to the reduction of s_k would be reduced by 1/2 of the initial knot-size in the melt.

A discrete further step of disknotting would occur by making an additional fold of the entanglement mesh-chain. This yields $m = 0$. Consequently, $s_k = 0$, which would correspond to a complete disappearance of the knot. In this case the distance between entanglements of the knot would be zero; $m = 0$ does not seem to be the probable case for normal spherulitic crystallization, but it will be the basis of annealing of PE at high pressures;

$m = 1$ seems the most probable for normal crystallization

$$s_k = m\, s_c/2 \,, \tag{38}$$

Fig. 16a shows this case

Equation (38) describes the dependence of s_k upon m. The areas F_k of the knot and F_e of the entanglements describe the amorphous zones. Hence, its molecules show an effective diameter d_a which is larger than the molecule diameter d_c within the crystal layer. The total two-dimensional unit cell of the knot, however, must be uniform in diameter. Hence, the thicker chains within the amorphous zone must incorporate during crystallization some holes, providing finally an effective thinning of the molecular monolayer to a diameter d_c. The areas of the two amorphous zones F_e and F_k have to be corrected under this point of view.

For the thickness reduced area of the knot results:

$$F'_k = f s_k \cdot d_a^2/d_c = b \cdot h_k \,, \tag{39}$$

where b is the width of the crystallite below the knot and h_k is the thickness of the knot as part of the amorphous layer.

From Eqs. (39) and (36) results:

$$h_k = 2\, s_k/(\sqrt{v} - m)(d_a/d_c)^2 \tag{40}$$

By substituting Eq. (38) into Eq. (40), one obtains:

$$h_k = \frac{m v^{5/4} d_a}{(\sqrt{v} - m)} \cdot \left(\frac{d_a}{d_c}\right)^2 \,. \tag{41}$$

Analogously, the cross-sectional area of the entanglement-layer above the crystal surface is calculated. The number of entanglements of the crystal surfaces within the unit cell is estimated to be equal to

$$N_e = b/2d_c \,. \tag{42}$$

b/d_c counts the number of chain segments with the length s_c that contributes to the crystal. The division by 2 stems from the fact that each entanglement is formed by two different chains. If

one inserts Eq. (36) in Eq. (42) and takes m equal to 1, then we obtain for $N_e = 25 \approx v$. The arc length of an entanglement on the crystal surface is estimated to be $2\pi n d_c$ (see also Appendix 2). The larger the value of n, the higher will be the degree of interpenetration of the entanglements on the crystal surface. Adjacent reentry of an entanglement arc (see Section 4.2) is excluded by taking $n \geq 1$.

Hence, for the van der Waals volume of an entanglement, we can write:

$$V_e = \underbrace{2\pi n d_c}_{\left(\begin{matrix}\text{arc}\\ \text{length}\end{matrix}\right)} \cdot \underbrace{d_a^2}_{\left(\begin{matrix}\text{cross-sectional area}\\ \text{of the "amorphous" molecule}\end{matrix}\right)} . \tag{43}$$

The area E of the d_c-mono-layer reduced entanglement arc can be calculated from V_e (Eq. (43)) and is equal to:

$$E = 2\pi n d_a^2 . \tag{44}$$

For the total area covered by entanglements, we obtain:

$$F'_e = v \cdot E = 2\pi n\, v d_a^2 . \tag{45}$$

The total thickness h_e of the two entanglement layer is given by

$$F'_e = b \cdot h_e ; \tag{46}$$

By substituting Eqs. (45) and (36) in Eq. (46), one obtains:

$$h_e = \frac{2\pi v n d_a^2}{f/2(\sqrt{v} - m)\, d_c} . \tag{47}$$

substituting Eq. (32) in (7), one obtains:

$$h_e = \frac{2\pi v^{1/4}}{(\sqrt{v} - m)} \cdot n \cdot \frac{d_a^2}{d_c} . \tag{48}$$

A somewhat more precise description of the thickness of the entanglement layer on the crystal suface is given in Appendix 2.

From expressions (41) and (48), one can calculate

$$l_a = h_k + h_e . \tag{49}$$

If use is made of the known values for v, d_a, and d_c and $m = 1$ in Eq. (41), one obtains for $h_k = 74.5$ Å.

Table 5 shows the values obtained for h_e as a function of n (Eq. (48)):

For $n = 1$, one obtains $h_k + h_e = 90{,}9$ Å, which corresponds to the experimental data $l'_{ac} = 90$ Å, (see Fig. 10) which characterize the percolation threshold of knots. The thickness of one entanglement-layer on the basis $n = 1$ is given by $h_e/2 = 8.2$ Å. This corresponds well to the estimation of the entanglement length from Appendix 2 ($h_e = 8{,}1$ Å).

The long period is given by:

$$L = l_a/(1 - \alpha) , \tag{50}$$

where α = volume fraction of crystallinity.

If L is multiplied by b, one obtains the area of the unit cell of the knot network in the semicrystalline state. This yields

$$L = R^2/b . \tag{51}$$

Due to the contraction by crystallization R decreases below the value s_c (13). The reduced value R_{red} can be calculated from the reduced volume of the monolayer crossection of the unit cell of the network.

$$R_{red}^2 \cdot d_c = \alpha y d_c^2 + (1 - \alpha) y d_a^2 , \tag{52}$$

where y is given by Eqs. (26, 30, 32)

$$\alpha = \frac{2\left(\frac{d_a}{d_c}\right)^2 - 1}{2\left[\left(\frac{d_a}{d_c}\right)^2 - 1\right]} - \sqrt{\left[\frac{2\left(\frac{d_a}{d_c}\right)^2 - 1}{2\left[\left(\frac{d_a}{d_c}\right)^2 - 1\right]}\right]^2 - \frac{\left(\frac{d_a}{d_c}\right)^2 - v^{-3/2}\left[2\pi n \frac{d_a}{d_c} + mv\left(\frac{d_a}{d_c}\right)^2\right]}{\left(\frac{d_a}{d_c}\right)^2 - 1}} , \tag{53}$$

Combining Eqs. (49, 50) with (51) and inserting, inspite of R^2, the value R_{red}^2, one obtains for α

Equations (41) and (48) for h_c and h_k and Eq. (53) for α completely determine the "unit cell" on the basis of the molecular parameters d_a, d_c, v, n, and m. The first three parameters are known.

Table 5. Thickness of the Entanglement-Layers on the Crystal Surfaces (Eq. (48))

n	h_e/Å
1	16.4
1.5	24.5
2	32.7

m and n are parameters of the knot model which were both taken as 1.

Equation (53) with $m = n = 1$ yields for α:

$\alpha = 75\%$

and L (eq. (50):

$L = 355$ Å ;

hence, we obtain for l_c:

$l_c = \alpha L = 266$ Å .

All data calculated from the model are confirmed well by experimental data for α and L of the slowly cooled series for $la'_c = 90$A (Fig. 10).

4.4.3. Morphological details of the calculated model: The formulae describing morphology for the special case of a molecular weight is $M = M'_c$, which means that an average chain is long enough to connect one knot to another. This describes the condition of percolation of the knots. On the other hand, crystal thickness is adopted as chain length between two entanglements:

$$l_c = s_c - 2l_s/2 \; . \tag{54}$$

When the known values for s_c and l_s (10, 3 A) are inserted, one obtains $l_c = 267$ A, which coincides well with the above value for l_c as calculated from Eq. (53) and L/Eq. (50).

The term $l_s/2$ characterizes the half arc which the chain contributes to the entanglement. It is seen that this conclusion is fulfilled experimentally in the case of slow cooling from the melt. This proves the model of a folded entanglement-mesh chain that forms the crystal.

When $m = 1$ (which includes crystallization-induced disknotting) and $n = 1$ (which includes desinterpenetration of the entanglements on the crystal surfaces), then

$l_a = 90$ A $= l'_{ac}$

can be derived. This means that the amorphous phase is formed by the knots. The coincidence of the calculated l_a with the experimental l'_{ac} indicates that knot concentration fulfills the percolation condition ($M = M'_c$). Values for $l_a < l'_{ac}$ for molecular weights smaller than M'_c are correlated to a decrease of knot concentration. The model model also involves a deformation of the unit cell of the knot-network (Fig. 16) by crystallization. Equation (52) indicates that the original equidistant distribution of knots given by $R_{red} = 274$ A for $\alpha = 0.75$ (in comparison with $R = s_c = 277$ A) is replaced to a longitudinal distance which corresponds to the longperiod ($L = 355$ A) and a lateral distance ($b = 212$ A) which describes the width of the unit cell of the knot-network (see Fig. 16). This anisometry comes from the growing crystals which do not stop before reaching an entanglement ($l_c \approx s_c$). The consequence is that the knots are slightly pushed in longitudinal direction (from original $R_{red} = 274$ A to $L = 355$ A).

The crystal growth is also responsible for the lateral contraction of the unit cell (from original $R_{red} = 274$ A to $b = 212$ A). Another consequence is the anisometry of the amorphous part within the unit cell of the knot network. The height is only $l_a = 90$ A, while the width is 212 A. This implies that the longitudinal shift of the knot is accompanied by a compression of the knot which must cause a preferential chain orientation within the amorphous phase perpendicular to the chain direction within the crystal (Fig. 16b). The dimensions of the crystal show an opposite anisometry: Its height ($l_c = 267$ A) is longer than the width ($b = 212$ A). The preferential perpendicular chain orientation in the amorphous phase is caused by taking $m = 1$ which describes a crystallization induced disknotting. Here, the preferential orientation of the amorphous phase is accompanied by an enhanced entanglement density within the amorphous zone ($s_k = s_c/2$). The existence of the width b of the unit cell could offer an explanation for the known mosaic bloc structure of crystalline lamellae.

In an isotropic semicrystalline polymer a perpendicular orientation of the amorphous phase is not detectable. It however becomes visible when the polymer is slightly ($\varepsilon \approx 50\%$) hot drawn. The spherulite structure in this case exhibits an affine deformation [30]. Then, an orientation of the crystals in draw direction and a perpendicular amorphous orientation f_{am} becomes detectable.

Samuels [30] calculated f_{am} from independent measurements of birefringence, density and sonic modulus of PP. Also in [31] a perpendicular orientation f_{am} of slightly drawn LDPE is detected. This is in support of the model presented here.

The knot model of the amorphous phase has some similarity with Pechold's meander model [32]. The amorphous phase in Pechold's model is given by the arcs of the meander. If these arcs would interpenetrate with each other, they would be similar to the knot-halves as shown in Fig. 16. The common feature of the meander model and the knot model is the vertical axis of symmetry which passes through the center of the meander on one hand, and through the center of the knot on the other hand. The meander model is the only one of the previous models of the amorphous phase which shows an analogy to the knot model. It is worth pointing out that the dimensions of the meander [32] and the "unit cell" of the knot network (see Fig. 16) are similar.

4.5. Mechanical properties

4.5.1. Elastic recovery of a semicrystalline polymer. If a semicrystalline polymer is deformed the first deformation mechanism involves a separation of lamellae. Amorphous layers are extended in this way. During this initial step of deformation crystallites act as strong elements. They represent multifunctional net-points which are connected by many tie molecules [24]. The elastic recovery $ER_x = 100\%$ when $x \leq 5\%$ (Fig. 7) is explained in this way. Following Fig. 16, knots form the center of the amorphous phase. Tie molecules which pass from one crystallite through another participate in these knots. Hence, similar to crystallites, the knots as force-bearing elements come into play.

Knots maintain a partial elastic recovery when crystals are plastically deformed above $x \approx 5\%$ (Fig. 7). In Figs. 3, 5, 6, 9 it is shown that the decrease of elastic recovery increases with the fraction of crystallinity. This is due to entropic elasticity of the stretching process of the chain segments with the length s_k within the knots. When x reaches 15% the plastic deformation of the lamellar structure comes to a saturation level. Elastic recovery ER_x for $15\% < x < 110\%$ (yield point, E_y) is maintained constant at approximately 60%. When the yield deformation E_y is surpassed, another type of plastic deformation occurs which is related to the formation of the fibrillar structure. This yields, similar to the situation of $x \approx 5\%$, another stepwise decrease of the elastic recovery. Elastic recovery of the solid state is hence strongly related to the state of the knot-network. Crystallites act as netpoints only at very low deformations. The influence of the crystallites on the elastic recovery can be completely discarded if the experiments are carried out several times [23]. In this case, only knots determine the elastic recovery.

4.5.2. Correlation to Peterlin's deformation model of semi-crystalline polymers According to the model of Peterlin [33], the initial lamellar structure is gradually transformed upon deformation into a fibrillar crystalline structure which characterizes the material after a necking process. A stack of lamellae is transformed hereby to a fibrillar structure which consists of microfibrils which themselves form fibrils. The microfibrils originate by cooperative micronecking processes from the lamellae. Each lamellae yields several microfibrils. The microfibrils represent the strongest element of the fibrillar structure. In spite of exhibiting alternating crystalline and amorphous blocks, they behave as needle-like crystals due to a large amount of intramicrofibrillar tie molecules which act across the amorphous blocks. The microfibrils are connected to each other by intermicrofibrillar tie-molecules, thus forming the fibrils.

Peterlin describes the deformation of the fibrillar structure by a shear displacement of the fibrils to each other and simultaneous shear displacements of the microfibrils to each other within the fibril. Fibrils slide more easily than do microfibrils within the fibril. Both processes lead to a dramatic increase of taut interfibrillar tie-molecules which yield the increased strength of the fibrillar structure. Layers of extended chains are formed in this way [33]. Simultaneously, the surface of the fibrils increases.

Let us visualize Peterlin's model in terms of the model of the amorphous phase as presented in section 4.4. (Fig. 16). Peterlin's interlamellar tie-molecules of the initial microspherulitic structure have to pass through the knots. This is evident from Fig. 16. The interlamellar tie-molecules are transformed by elongation below the melting

point into the inter (micro) fibrillar tie-molecules. This corresponds well to the model of microfibril formation from the melt state [17, 28] : when a knot-mesh is stretched a fiber crystal is formed. Two stable multifunctional knots at the ends of the microfibril maintain the stretched state in the melt and allow a transfer to the solid state by cooling down the melt. An analogous mechanism will describe the microfibril formation in the solid state. Figure 17 offers a simplified model.

When the knot-mesh is stretched these entanglement-meshes are aligned in the stretch-direction as shown in Fig. 17. The total deformation of the entanglement and knot-network is given by the extensibility of the knot-mesh as well as by the extensibility of the entanglement-mesh. The right-hand side of Fig. 17 shows the completely extended structure. Due to the multi-functionality of the knots more than only one stretched entangled

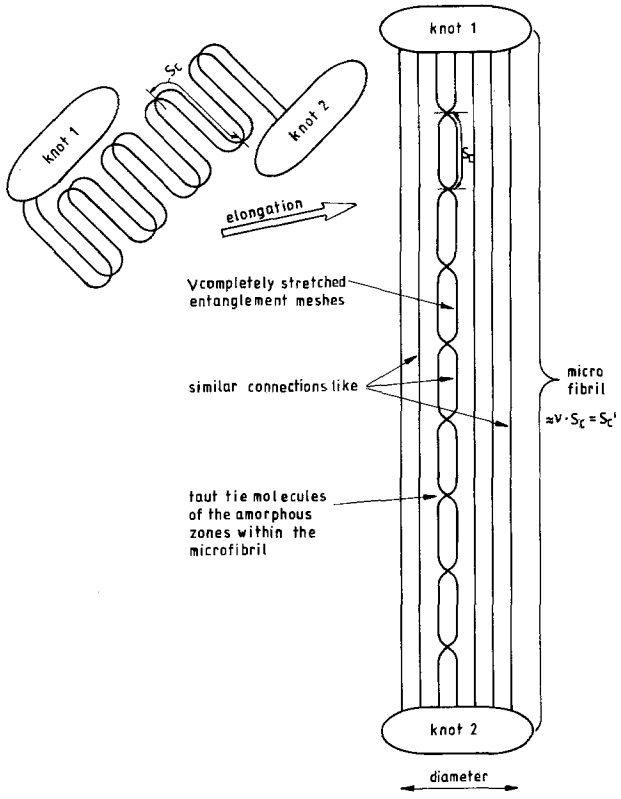

Fig. 17. Schematic drawing for the transformation of the lamellar structure (left) of isotropous polyethylene to the microfibrillar structure (right) by solid state drawing. Fibril lengths $\approx s_c' = \nu\, s_c = 7500$ A;

chain will pass from knot to knot. Peterlin's model of the transformation of interlamellar tie-molecules to intermicrofibrillar tie-molecules can hence be explained in a simple manner by the stretching of a knot-mesh. The stretched entanglement-meshes within the stretched knot-mesh (microfibril) form the crystallites within the microfibril. The entanglements at the ends of the stretched entanglement-meshes within the stretched knot-mesh (Fig. 17) form the amorphous phases within the microfibril. Peterlin considers intramicrofibrillar tie-molecules which connect the crystallites of the microfibril to a strong "needle-like" crystal. This preferential strength of the amorphous blocks within the microfibril is also described easily by the present model. Here, the amorphous phase consists mainly of entanglements, but does not contain knots. Thus, these amorphous phases must be much smaller and stronger than the amorphous phases which connect the microfibrils. The latter ones contain knots and hence are much thicker and softer. Peterlin's differentiation between intra and inter (micro) fibrillar molecules is easily explained by amorphous phases formed by entanglements or knots.

Following Peterlin, still more complex superstructures exist in the stretched solid state. Microfibrils form fibrils. The fibrils are easier to deform than the strong microfibrils. The fibril itself however is separated by still softer regions of chain molecules. This is explained well by the situation of polymers with a chain length below M_c'. Islands of knot-meshes exist which do not cohere [17].

When the islands are stretched they then form the fibrils. Every stretched mesh of the knot-network-island forms a microfibril. The islands are separated from each other by unknotted molecules. These molecules have, of course, the maximum flexibility and represent the easily sliding matrix which separates the fibrils from each other.

Baltá and Peterlin made their investigations on polypropylenes with $M < M_c'$ [34, 35] $M_c' \approx 470\,000$ (see data from [36]).

At molecular weights above M_c' a differentiation between microfibrils and fibrils no longer has sense. Above M_c' only microfibrils will exist.

In the present work it has been shown that Peterlin's model of microfibrils and fibrils is a direct consequence of a complete stretching of a network of knots and entanglements in a case where

the knot-network does not percolate. This is the case for most of the thermoplastic materials.

4.5.3. Relation to Kilian's van-der-Waals-Network theory: Kilian's van der Waals Network theory has been applied to various polymer system with success [24, 37]. This theory describes accurately the force strain behavior in elongation as well as in compression. The principal parameter is "λ_m" which characterizes the maximum extensibility of a mean mesh of the network. A parameter "a" characterizes the energetic interaction of the chain molecules. Hence, "a" is related to the functionality of the net-points of the network. A third parameter is the entropy invariant unit"M_u". In every application of the van der Waals Network Theory for Polyethylenes M_u is taken as 14 which equals the molecular weight of the CH_2-group.

The extensibility of an entanglement-mesh yields:

$$\lambda_m = \lambda_c = \sqrt{s_c/l}\,, \tag{55}$$

where l is the length of the entropy invariant unit. When l (following Kilian's definition for the strain invariant) is taken as 1.27 Å (projected length of the C–C bond) and $s_c = 278$ Å (see section 4.3.) it yields: $\lambda_c = \sqrt{278\text{ Å}/1.27\text{ Å}} = 14.8$.

In Section 4.3.1, however, it is shown that λ_c is only 5.2. If in Eq. (55) a value of $l_s = 10{,}3$ Å (see Section 4.3.) would be used instead of the value of $l = 1.27$ Å used by Kilian, then a value $\lambda_c = 5.2$ would be obtained.

In what follows, an attempt to justify the statistical chain segment l_s as a proper mechanically effective invariant of deformation is made. If l_s is considered as entropy invariant of deformation, this implies that the 8 CH_2-groups forming the statistical chain segment are considered as a rigid, undeformable part of the molecule. This, of course, is not the case. A real C_8H_{16}-segment is flexible, but it is not random at its ends. If the chain grows above 8 CH_2-groups the additional carbon atoms are correlated to the orientation of the endgroups of the real C_8H_{16} segments. The concept of the statistical chain segment, however, takes out all flexibility of the C_8H_{16} segment and concentrates it at the end of the resulting stiff segment. The next (rigid) C_8H_{16} segment then has a completely random orientation with respect to the reference segment. This means that the artificial construction of a statistical chain segment is a mechanically effective unit (Eqs. (4), (5)). On the other hand, van der Waals network theory requires λ_m-values of ≈ 15 for crystalline HDPE samples [37]. As mentioned before, a percolating knot network exhibits the extensibility $\lambda'_c = v = 27$

The knot-network hence exhibits a deformability which is above the previously cited λ_m-value of ≈ 15, $\lambda'_c = 27$ represents a maximum value.

Peterlin and Baltá [35] as well as Peterlin and Corneliussen [38] mention that the long period of the fibrillar structure is characterized only by drawing temperature. It has nothing to do with the long period of the initial structure. This is explained by a melting process of the initial structure on heterogeneous drawing. The long period of the fibrillar structure is hence given by the temperature when the material recrystallizes. Crystalline thickness is hereby controlled. If one considers that entanglement-density is not changed by the crystallization process, this implies that at low crystalline thickness a lot of chain-folds must be introduced. This chain-folding process is super-imposed to a stretching of the network. Hence, an effective reduction of λ_c will result. This might be the reason why by applying Kilian's van der Waals network theory lower values for λ_m than $\lambda'_c = 27$ are observed.

Conclusions

The structure of the melt is described as a fluctuating network of entanglements. The longest entangled chains form entanglements with each other. These entanglements of a "entanglement mesh chain" are called knots. They are "spider"-like as in multifunctional netpoints. A knot-network acts as a superstructure of an entanglement network. The question arises as to how this superstructure acts during crystallization from the melt state. A model contains the following features:

- the existence of a crystallization-induced disknotting;
- the formation of "folds" of the above-described entanglement-mesh chain during crystallization. This model is based on the simultaneous stretching of an entanglement mesh during crystallization while the spatial distribution of the knots remains unchanged;

- the formation of the amorphous phase by the knots;
- the amorphous phase - due to the disknotting process - exhibits a preferential orientation perpendicular to the crystallites.

Calculations based on this model explain quantitatively the morphological data of slowly cooled linear polyethylene with a molecular weight that corresponds to the percolation threshold of the knots. The critical thickness of the amorphous phase $l'_a = 90A$ at $M = M'_c$ is explained by this model. Other morphological parameters like crystallinity and long period L can likewise be calculated. The model does not involve disentanglement by crystallization. This is the reason why the morphology of a slowly cooled polyethylene sample with $M = M'_c$ is described so well. The morphological data can be derived on the basis of three independent parameters: a) chain flexibility α, b) Rault's degree of interpenetration v describing the behavior of the amorphous phase, and c) crystalline density ρ_c describing the crystalline phase.

It is shown that Peterlin's model of yielding of thermoplastic materials can be derived from the knot model. On the other hand Kilian's van der Waals Network Theory requires an extremely small invariant of deformation for the chains which form the network. It is finally shown that a network of entanglements with a knot network as superstructure can easily explain the maximum extensibility of a network, while at the same time the mechanical effective statistical unit does not deviate too much from the statistical chain segment. The assumption of a knot network in a thermoplastic melt thus explains satisfactorily both morphology and mechanical properties in the solid state.

Acknowledgements

Grateful acknowledgement is due to Prof. Dr. F.J.Baltá-Calleja for many helpful and interesting discussions and his kind advice and encouragement on this work. Prof. Dr. H.G. Kilian is thanked for a critical review of this paper, presented in July 1992 at the university of Ulm. The author also is grateful to the sabatical program of the Ministerio de Educacion y Cienca (Spain). Thanks are due to the Deutsche Forschungsgemeinschaft, as well as to the Bundesministerium für Forschung und Technologie (FRG) and the Ministerio de Asuntos Exteriores and CAICYT (Spain) for generous support of this project. I wish to thank BASF and Hoechst AG for providing the investigated samples. Many thanks are expressed to Christa Bayer for improving and typing this text.

Appendix 1

In Section 4.3.1 it is shown that the extensibility λ_c of an entanglement mesh is given by

$$\lambda_c = \sqrt{v} \,. \tag{2}$$

We now calculate the smallest chain length xl_s which obeys Eq. (2):

$$\lambda_c = \sqrt{v} = \sqrt{x \cdot l_s / l_u} \,. \tag{A1}$$

l_s in eq. (A1) is counted in CH_2-units $(l_u) \cdot (l_s/l_u \approx 8$ see Appendix 2).

From Eq. (A1) $x \cdot l_s$ can easily be calculated as $v \cdot l_u$:

$$x \cdot l_s = v \cdot l_u \,. \tag{A2}$$

Following Eq. (A1), the $v \cdot l_u$ chain segment counts as mechanically independent from the next $v \cdot l_u$-unit. Hence, it seems understandable that electric potentials of CH_2-groups farther away than $v \cdot l_u$-units can no longer influence the rotational potential of the reference CH_2-group. Thus, it seems reasonable that $N = v$ holds for the c_N-value of a molecule in an entangled melt.

Appendix 2

Precise shape of an entanglement on the surface of the crystal

The precise shape of the smallest arc which can form an entanglement is given in Fig. A1.

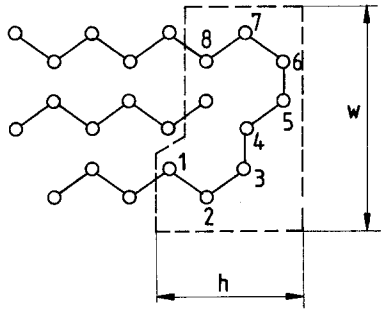

Fig. A1. Realization of an entanglement arc of Fig's. 12 and 16 by the zig-zag chain of PE without bending the bond angle

Its centerline is given by the 8 CH_2-groups which characterize the mechanical effective statistical chain segment: $8 \cdot 1.27$ Å $= 10.2$ Å $\approx l_s$.

The outer length s_b of the entanglement arc is given by the sum of the distances plus 2/2 of the diameter d_a of the molecule:

distance 1–2:	1.27 Å	(projected length of the C–C-bond)
2–3:	1.27 Å	
3–4:	1.54 Å	(length of the C–C-bond)
4–5:	1.27 Å	
5–6:	1.54 Å	
6–7:	1.27 Å	
7–8:	1.27 Å	
d_a:	4.26 Å	
$s_b =$	13.69 Å ,	

which corresponds well to the approximation $s_b = \pi d_a = 14.19$ Å (from Eq. (44)). Analogously, the width w of an entanglement is calculated to be:

distance	2–3	1.27 Å
	3–4	1.54 Å
	4–5	1.27 Å
	5–6	1.54 Å
	6–7	1.27 Å
	d_a	4.26 Å
	$w =$	11.2 Å

For the height $h_e/2$ of an entanglement, it follows that:

distance	1–2	1.27 Å
	2–3	1.27 Å
distance	3–4	0
distance	4–5	1.27 Å
	d_a	4.26 Å
	$h_e =$	8.1 Å

Summary of all parameters

ER_x	elastic recovery after initial deformation of x%
λ_B	elongation at break
λ_o	draft
λ_{oB}	elongation at break of the melt
Δn	birefringence
L	long period
ρ_c	density of the crystalline phase
ρ_a	density of the amorphous phase
d_c	effective thickness of a molecule in the crystalline phase
d_a	effective thickness of a molecule in the amorphous phase
l_c	crystal thickness
l_a	thickness of the amorphous layers
α	volume degree of crystallinity
l'_{ac}	thickness of the amorphous layer when knots percolate
M	molecular weight
M_η	viscosimetric average of the molecular weight
M_w	weight average of the molecular weight
M_u	molecular weight of the monomer
l	bond-length
l_u	projected length of the monomer
l_s	length of the statistical chain segment
M_c	critical entanglement molecular weight
M'_c	critical knot molecular weight
s_c	curvilinear distance between entanglements
s'_c	curvilinear distance between knots
s_k	curvilinear distance between entanglements within a knot
ζ	distance between entanglements
R, R_{red}	distance between knots
v	Rault's degree of interpenetration of an entanglement-mesh
α	chain flexibility
C_N, $C_{N\infty}$	Flory's chain flexibility
λ_c	extensibility of an entanglement-mesh
λ'_c	extensibility of a knot-mesh
λ_k	intrinsic extensibility of a knot-mesh
λ_m	extensibility of a representative mesh in Kilian's van der Waals-network theory.
f	functionality of a knot
y	total chain length within the two-dimensional projection of the unit cell of the knot network
$P^{(1)}$, $P^{(2)}$, $P^{(3)}$	length of the 1-, 2- or 3-dimensional projection of the statistical chain between two knots
b	width of the unit cell of the knot network
h_e, F_e	thickness resp. cross-sectional area of the entanglement layers on the crystal surfaces
h_k, F_k	thickness resp. cross-sectional area of the knot in the semi-crystalline unit cell of the knot-network.

F_c	cross-sectional area of a crystal within the unit cell of the knot-network
m,n	numbers describing the knot-model
N	number of CH_2-groups of a PE-chain

References

1. Wunderlich B (1973) Macromolecular Physics. N.Y. Academic Press, London
2. Keller A (1985) In: Selácek B (ed) Morphology of Polymers, Prac. 17th Europhys Conf Macromol Phys. Berlin de Gruyter, Berlin (1986)
3. Hoffmann JD, Lauritzen JI (1961) J Res Nat Bur Stand 65 A: 297
4. Sanchez IC (1975) J Macromol Sci 12:113
5. Fischer EW (1985) Integration of Fundamental Polymer Science and Technology, L.A. Kleintjens and P.J. Lemstra (Eds.) Elsevier Applied Science Publishers, London & NY, 456
6. Fischer EW (1978) Pure Appl Chem 50:1319
7. Stamm M, Fischer EW, Dettenmaier M (1979) P. Covert Farad Disc Chem Soc 68:263
8. Rault J, Sotton M, Rabourdin C, Robelin E (1980) J de Physique 41:1459
9. Robelin E, Rousseaux F, Lemonnier M, Rault J (1980) J de Physique 41:1469
10. Rault J, Robelin E (1982) J de Physique 43:1437
11. Rault J, Robelin E, Perez G (1983) J Macromol Sci Phys B 22(4):577
12. Rault J (1986) C R C Critical Reviews in Solid State and Materials Sciences 13:57–93 C R C Press Inc
13. Holl B, Heise B, Kilian HG (1983) Colloid Polym Sci 261:978–992
14. Heise B, Kilian HG, Wulff W (1979) Progr Colloid Polym Sci 67:263
15. Katayama K, Amano T, Nakamura K (1968) Kolloid Zeitschrift und Z f Polymere, Bd226. Heft 2:12521
16. Bayer RK (1991) Colloid Polym Sci 269:421–432
17. Bayer RK, Liebentraut F, Meyer T (1992) Colloid Polym Sci 270:331–348
18. Discussion with Baltá-Calleja FJ
19. Bayer RK, Baltá-Calleja FJ, Kilian HG (to be published)
20. Rault J, Robelin-Souffache E (1989), J Polymer Sci B, Vol 27:1349
21. Capaccio G, Crompton TA, Ward IM (1976) J of Polymer Sci Polymer Phys Ed Vol. 14:1641–1658
22. Mayer J, Schrödi W, Heise B, Kilian HG (1990) Acta Polymerica Nr. 7:363–370
23. Bayer RK, Knoche G, Sammet D, Wilken D, Schlimmer M (1993) Plaste und Kautshcuk 7:234–243
24. Paul E, Heise B, Schrödi W, Kilian HG (1991) Progr Colloid Polym Sci 85:12–22
25. Rault J (1985) C R Acad Sc Paris, t.300 Serie II, no. 10:433–436
26. Comment of the referee of Colloid Polym Sci
27. Schultz J (1974) Polymer Materials Sci, Prentice Hall, Englewood Cliffs N.J., p 224
28. Bayer RK, Baltá-Calleja FJ, Lopez Cabarcos E, Zachmann HG, Paulsen A, Brüning F, Meins W (1989) J of Materials Sci 24:2643–2652
29. Flory PJ (1969) Statistical Mechanics of Chain Molecules John Wiley & Sons, N.Y.London, Sydney, Toronto
30. Samuels RJ (1965) J Pol Sci Part A, Vol 3:1741
31. Hoshino S, Powers J, LeGrand DG, Kawai H, Stein RS (1962) J Pol Sci 58:185
32. Pechold WR, Grossmann HP (1979) Disc Faraday Soc 68:58–77
33. Peterlin A (1975) Colloid Polym Sci 253, No. 10:809–823
34. Meinel G, Morosoff N, Peterlin A (1970) J Pol Sci Part A 2, Vol. 8:1723–1740
35. Baltá-Calleja FJ, Peterlin A (1970) J Macromol Sci Phys B 4(3):519–540
36. Prox M (1993) Thesis Univ Erlangen FRG
37. Kilian HG, Schrödi W, Ania F, Bayer RK, Baltá-Calleja FJ (1991) Colloid Polym Sci 269:859–866
38. Corneliussen R, Peterlin A (1967) Angewandte Makromol Chemie 105:193

Received January, 4, 1993;
accepted December 21, 1993

Author's address:
Dr. R.K. Bayer
Universität Kassel
Institut für Werkstofftechnik
Mönchebergstr. 3
34125 Kassel